Supporting Information

Development of Shape-Tuned, Monodisperse Block Copolymer Particles through Solvent-Mediated Particle Restructuring

Jae Man Shin[1], Young Jun Lee[1], Mingoo Kim[1], Kang Hee Ku[1], Junhyuk Lee[1], YongJoo Kim[2], Hongseok Yun[1], Kin Liao[3], Craig J. Hawker[,4] and Bumjoon J. Kim*[,1,2]*

[1] Department of Chemical and Biomolecular Engineering, [2] KAIST Institute for NanoCentury, Korea Advanced Institute of Science and Technology (KAIST), Daejeon 34141, Republic of Korea

[3] Department of Mechanical Engineering, Khalifa University, Abu Dhabi, United Arab Emirates

[4] Materials Research Laboratory, University of California, Santa Barbara, California 93106, United States

*E-mail: bumjoonkim@kaist.ac.kr (B. J. K.)

*E-mail: hawker@mrl.ucsb.edu (C. J. H)

Optimization of Membrane Emulsification for Generation of BCP Spheres

Herein we describe the optimization process to produce monodisperse BCP spheres using PS-*b*-P4VP as an example. First, the selection of an appropriate organic solvent for the disperse phase is important, since the favorable interactions between P4VP units and silanol groups on the membrane surface can affect the wettability during emulsification.[1,2] Monodisperse particles were obtained by using toluene as a PS-selective solvent for PS-*b*-P4VP,[3] where the formation of P4VP-core micelles in the disperse phase effectively screened the P4VP-silanol interactions (**Figures S1(a-c)**). On the other hand, the use of chloroform, a less selective solvent for PS-*b*-P4VP, as a disperse phase led to polydisperse particles. This is attributed to the increased wettability of the membrane by favorable interaction of the membrane surface and P4VP chains, which might induce coalescence of the organic phase while passing through the membrane pore (**Figures S1(d-f)**).

Second, the operation pressure (P) for membrane emulsification should be optimized for achieving monodispersity of the generated droplets, which has been demonstrated in our previous work.[4] For the case of a d_{pore} = 1.1 μm membrane, the critical pressure (P_c) was measured to be 15 kPa. A series of BCP particles were prepared at different P/P_c values from 1.33 to 1.67, and 2.67 (**Figure S2**). It was shown that increase of the P/P_c resulted in the increase of particle diameter and coefficient of variation (CV, defined as a standard deviation divided by average particle diameter) values. More than 200 particles from the SEM images were characterized to obtain CV value. The best monodispersity of the particles (i.e., CV < 15 %) was attainable at P/P_c = 1.33, and such pressure conditions were used throughout this work.

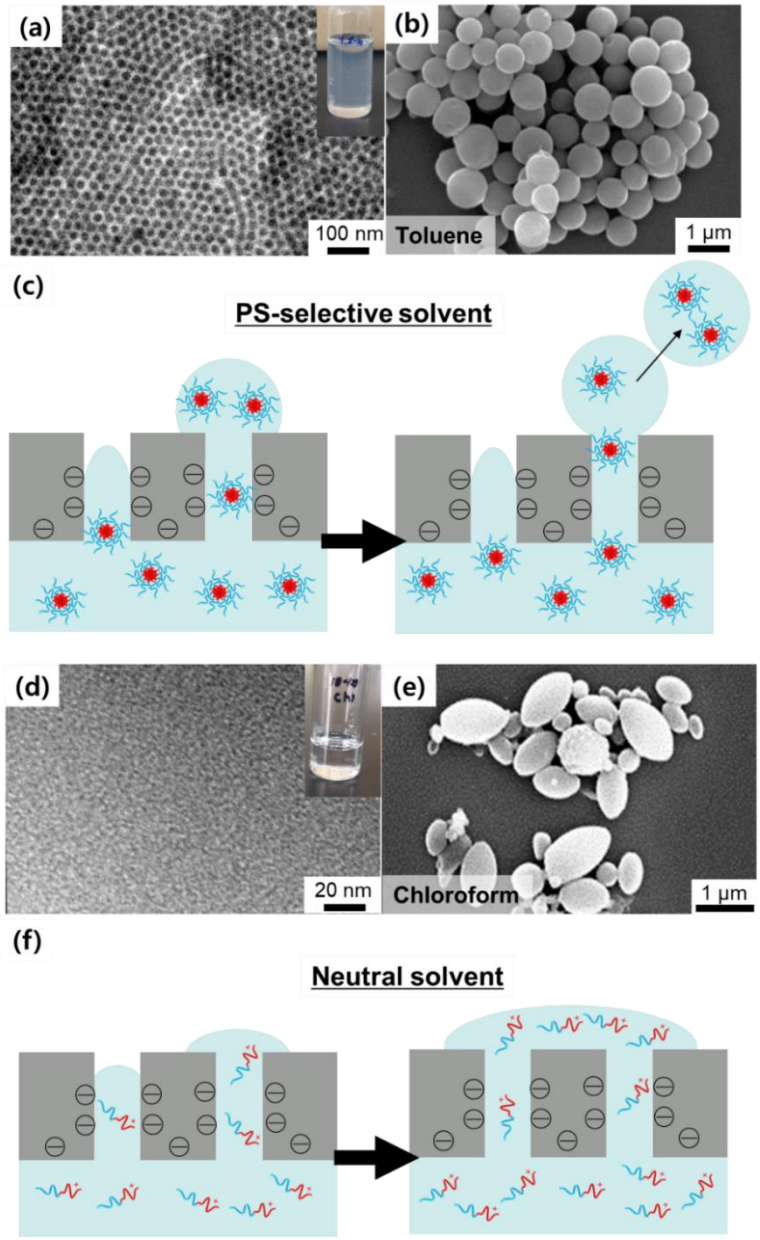

Figure S1. (a) TEM image of spherical micelles of PS_{10k}-*b*-$P4VP_{10k}$ on the film, which was cast from the polymers in toluene (3 mg/ml). (b) SEM image of PS_{10k}-*b*-$P4VP_{10k}$ particles emulsified by SPG membrane (d_{pore} = 1.1 μm) using toluene. (c) Schematic illustration showing the successful formation of monodisperse droplets using PS-selective solvents by efficiently screening the interaction between the P4VP and silanol membrane surface. (d) TEM image of PS_{10k}-*b*-$P4VP_{10k}$ on the film, which was cast from the polymers in chloroform (3 mg/ml). (e) SEM image of PS_{10k}-*b*-$P4VP_{10k}$ particles emulsified by SPG membrane (d_{pore} = 1.1 μm) using chloroform. (f) Schematic illustration showing the coalescence of droplets at the membrane surface using neutral solvents, due to interaction between the P4VP and silanol membrane surface.

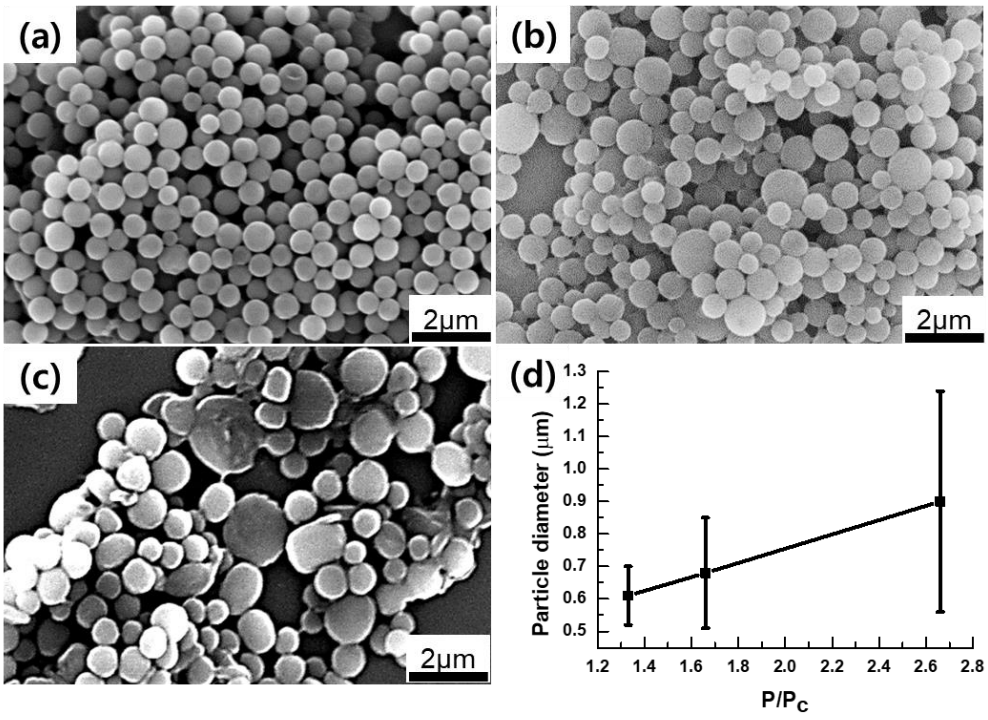

Figure S2. (a-c) SEM images of PS_{10k}-*b*-$P4VP_{10k}$ particles emulsified using a d_{pore} = 1.1 μm SPG membrane at (a) P/P_c = 1.33 (P = 20 kPa), (b) P/P_c = 1.67 (P = 25 kPa), and (c) P/P_c = 2.67 (P = 40 kPa). The PVA concentration in the continuous phase was fixed to 10 mg/mL. (d) Plot of particle diameters as a function of P/P_c, where the error bars indicate standard deviation.

Optimization of Dual Surfactants for Neutral Surrounding Conditions for Reshaping BCP Spheres to Ellipsoids

To generate a neutral wetting condition of both blocks to the surrounding aqueous phase, the choice of dual surfactant mixtures and their mixing ratios were optimized. For symmetric PS_{16k}-*b*-$PDMS_{17k}$, a mixture of SDS and PVA was used as a dual surfactant system where SDS is selective to the PS block while PVA is selective to the PDMS block. Therefore, the weight ratio of SDS:PVA was varied from 1:2 to 1:1 and 2:1, and the resulting particle morphology was observed. At the SDS:PVA = 1:2, a mixture of onion particles (with PDMS outermost layer) and prolate ellipsoids was observed in the batch, while SDS:PVA = 2:1 samples contained a mixture of onion particles (with PS outermost layer) and prolate ellipsoids. By contrast, SDS:PVA = 1:1 was a neutral condition where full transformation to prolate ellipsoids in the batch was achieved (**Figure S3**). For lamellae-forming PS_{34k}-*b*-PB_{25k}, SDS and PVA favorably interact with the PB and PS blocks, respectively. We also observed that the weight ratio of SDS:PVA = 1:1 is optimal one to transform all of the particles to ellipsoids (**Figure S4**). For PS_{10k}-*b*-$P4VP_{10k}$, a combination of CTAB and HO-CTAB surfactants was used, where each surfactant favorably interacts with either the PS or P4VP block, respectively.[5,6] To find the optimal weight ratio of CTAB:HO-CTAB, the weight ratios were varied from 1:1 to 1:2 and 1:4. At the ratio of 1:2, all the particles were transformed to ellipsoids while 1:1 and 1:4 ratios showed incomplete transition to prolate ellipsoids **(Figure S5)**. Additionally, the optimal weight ratio of the dual surfactants for generating neutral surrounding condition for cylinder-forming BCPs (PS_{31k}-*b*-$PDMS_{17k}$, PS_{35k}-*b*-PB_{11k}, and PS_{15k}-*b*-$P4VP_{7k}$) was determined similarly. For PS_{31k}-*b*-$PDMS_{17k}$ and PS_{35k}-*b*-PB_{11k}, the weight ratio of SDS:PVA = 2:1 was a neutral surrounding, at which all the particles transformed to oblates ellipsoids. For PS_{15k}-*b*-$P4VP_{7k}$, the CTAB:HO-CTAB = 1:1 was required to produce oblate ellipsoids.

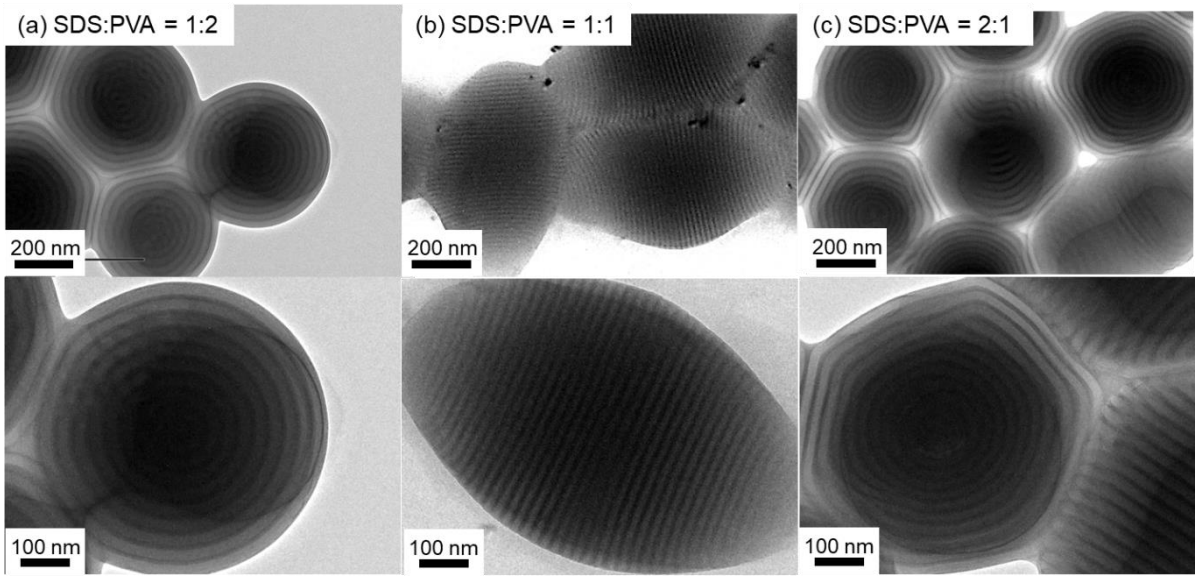

Figure S3. TEM images of PS_{16k}-*b*-$PDMS_{17k}$ BCP particles after chloroform annealing with varying SDS:PVA weight ratios of (a) 1:2, (b) 1:1, and (c) 2:1. Overall surfactant concentration was fixed to 3 mg/mL.

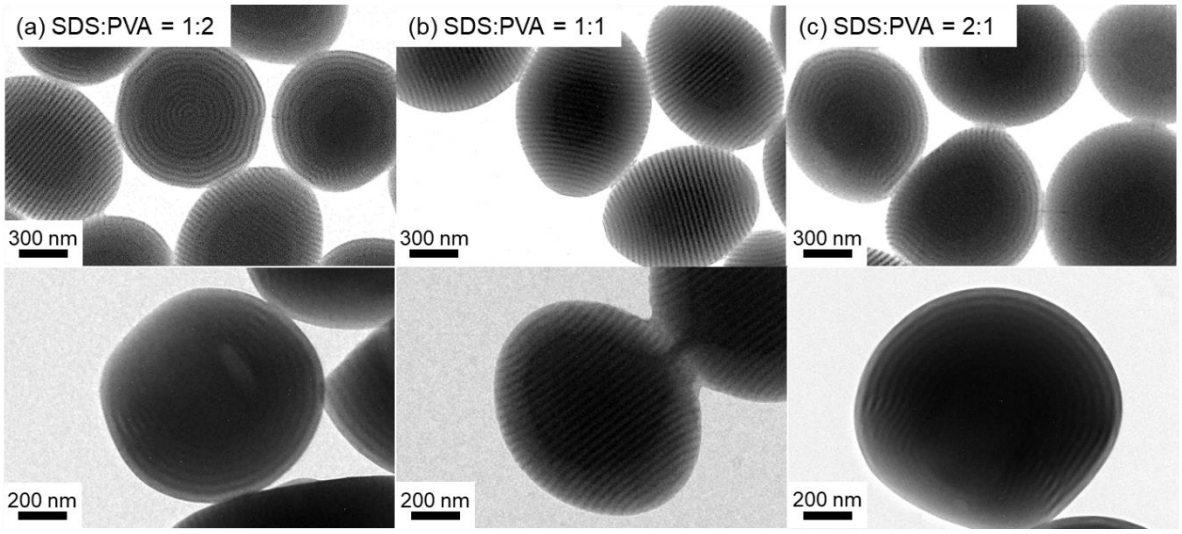

Figure S4. TEM images of PS_{34k}-*b*-PB_{25k} BCP particles after chloroform annealing with varying SDS:PVA weight ratios of (a) 1:2, (b) 1:1, and (c) 2:1. Overall surfactant concentration was fixed to 3 mg/mL. PB domain appear dark due to OsO_4 staining.

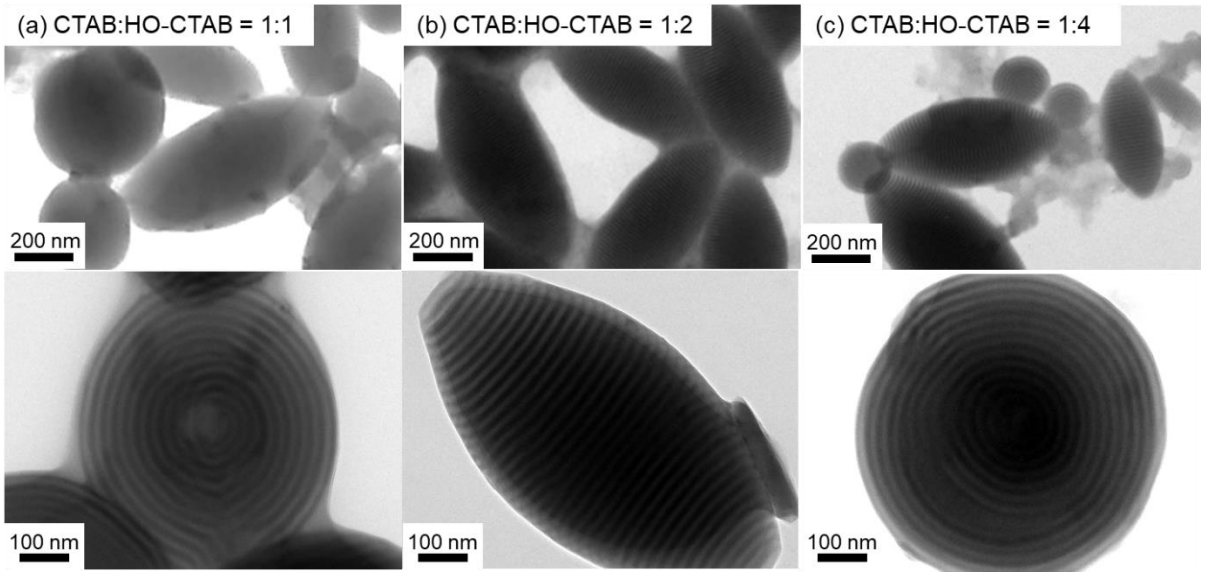

Figure S5. TEM images of PS_{10k}-*b*-$P4VP_{10k}$ BCP particles after chloroform annealing with varying CTAB:HO-CTAB weight ratios of (a) 1:1, (b) 1:2, and (c) 1:4. Overall surfactant concentration was fixed to 3 mg/mL. P4VP domain appear dark due to I_2 staining.

Table S1. Summary of particle size information.

	BCP	d_{pore} (μm)	Before (spheres)	After (prolate and oblate ellipsoid)		
			Diameter (μm) (CV (%))	Major Axis (μm) (CV (%))	Minor Axis (μm) (CV (%))	Aspect Ratio (AR)
Lamellae-forming BCPs	PS_{10k}-*b*-$P4VP_{10k}$	5.1	2.48±0.28 (11.2)	4.45±0.52 (11.7)	1.89±0.22 (11.6)	2.35
		2.1	1.09±0.12 (11.0)	2.25±0.35 (15.5)	0.93±0.12 (12.9)	2.41
		1.1	0.61±0.08 (13.1)	1.19±0.17 (14.2)	0.58±0.07 (12.0)	2.07
		0.5	0.33±0.04 (12.1)	0.65±0.12 (18.4)	0.34±0.06 (17.6)	1.89
	PS_{16k}-*b*-$PDMS_{17k}$	5.1	3.00±0.31 (10.3)	4.68±0.42 (9.0)	2.57±0.24 (9.3)	1.82
		2.1	1.10±0.12 (10.9)	1.97±0.19 (9.6)	1.12±0.11 (9.8)	1.74
		1.1	0.59±0.06 (10.2)	1.36±0.15 (11.0)	0.88±0.09 (10.2)	1.55
		0.5	0.30±0.03 (10.0)	0.49±0.06 (11.1)	0.34±0.04 (11.7)	1.44
	PS_{34k}-*b*-PB_{25k}	5.1	2.56±0.24 (9.4)	3.05±0.36 (11.8)	2.32±0.22 (9.4)	1.31
		2.1	1.03±0.09 (8.7)	1.94±0.20 (10.3)	1.39±0.14 (10.1)	1.28
		1.1	0.62±0.06 (9.7)	1.00±0.11 (11.0)	0.78±0.08 (10.2)	1.28
		0.5	0.29±0.03 (10.3)	0.55±0.05 (9.1)	0.46±0.04 (8.7)	1.18
Cylinder-forming BCPs	PS_{15k}-*b*-$P4VP_{7k}$	5.1	2.35±0.23 (9.8)	4.98±0.47 (9.4)	1.04±0.09 (7.9)	4.38
		2.1	0.93±0.11 (11.8)	1.75±0.27 (15.4)	0.43±0.05 (11.6)	3.50
		1.1	0.54±0.06 (11.1)	0.98±0.15 (15.3)	0.33±0.04 (12.1)	3.01
		0.5	0.31±0.03 (9.7)	0.52±0.09 (17.3)	0.25±0.04 (16.0)	2.06
	PS_{3k}-*b*-$PDMS_{17k}$	5.1	2.44±0.21 (8.6)	4.08±0.43 (10.5)	1.02±0.13 (12.7)	4.01
		2.1	1.05±0.12 (11.4)	2.03±0.17 (8.4)	0.67±0.05 (7.5)	3.03
		1.1	0.71±0.07 (9.9)	1.04±0.10 (9.6)	0.41±0.04 (9.8)	2.53
		0.5	0.27±0.04 (14.8)	0.43±0.07 (16.3)	0.26±0.04 (15.4)	1.66
	PS_{35k}-*b*-PB_{11k}	5.1	2.56±0.24 (9.4)	2.74±0.31 (11.3)	1.51±0.19 (12.7)	1.81
		2.1	1.07±0.09 (8.4)	1.10±0.14 (12.8)	0.82±0.11 (14.2)	1.35
		1.1	0.62±0.06 (9.7)	0.71±0.08 (11.2)	0.59±0.07 (11.8)	1.23
		0.5	0.29±0.03 (10.3)	0.31±0.05 (16.1)	0.28±0.03 (10.7)	1.11

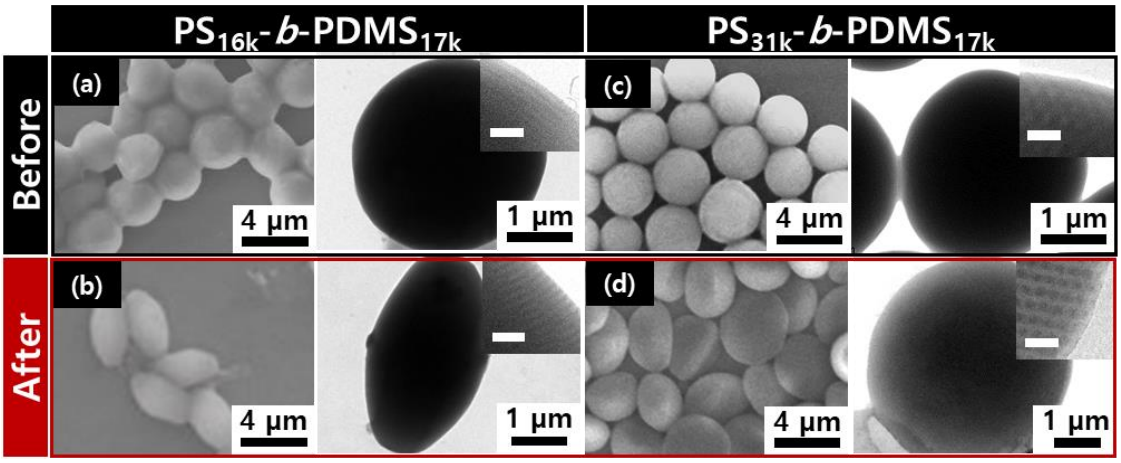

Figure S6. SEM and TEM images of (a) PS_{16k}-*b*-$PDMS_{17k}$ and (c) PS_{31k}-*b*-$PDMS_{17k}$ spheres produced from membranes with d_{pore} = 5.1 μm. The particles were transformed to (b) prolate ellipsoids and (d) oblate ellipsoids by PRSE. Scale bars in the insets (white) are 100 nm.

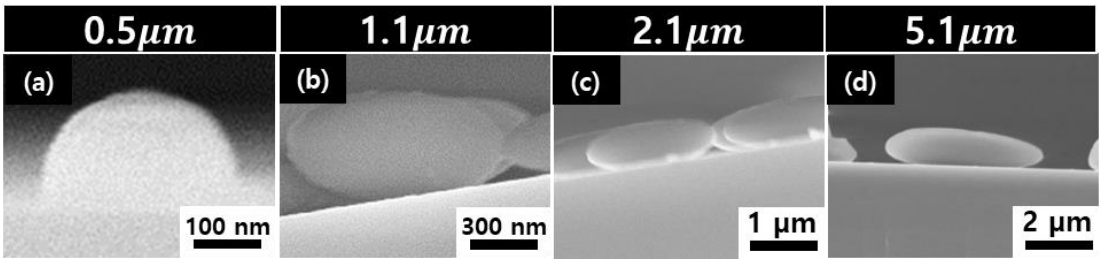

Figure S7. Side-view SEM images of PS_{31k}-*b*-$PDMS_{17k}$ oblate ellipsoids produced from membranes with d_{pore} = (a) 0.5, (b) 1.1, (c) 2.1 and (d) 5.1 μm after PRSE.

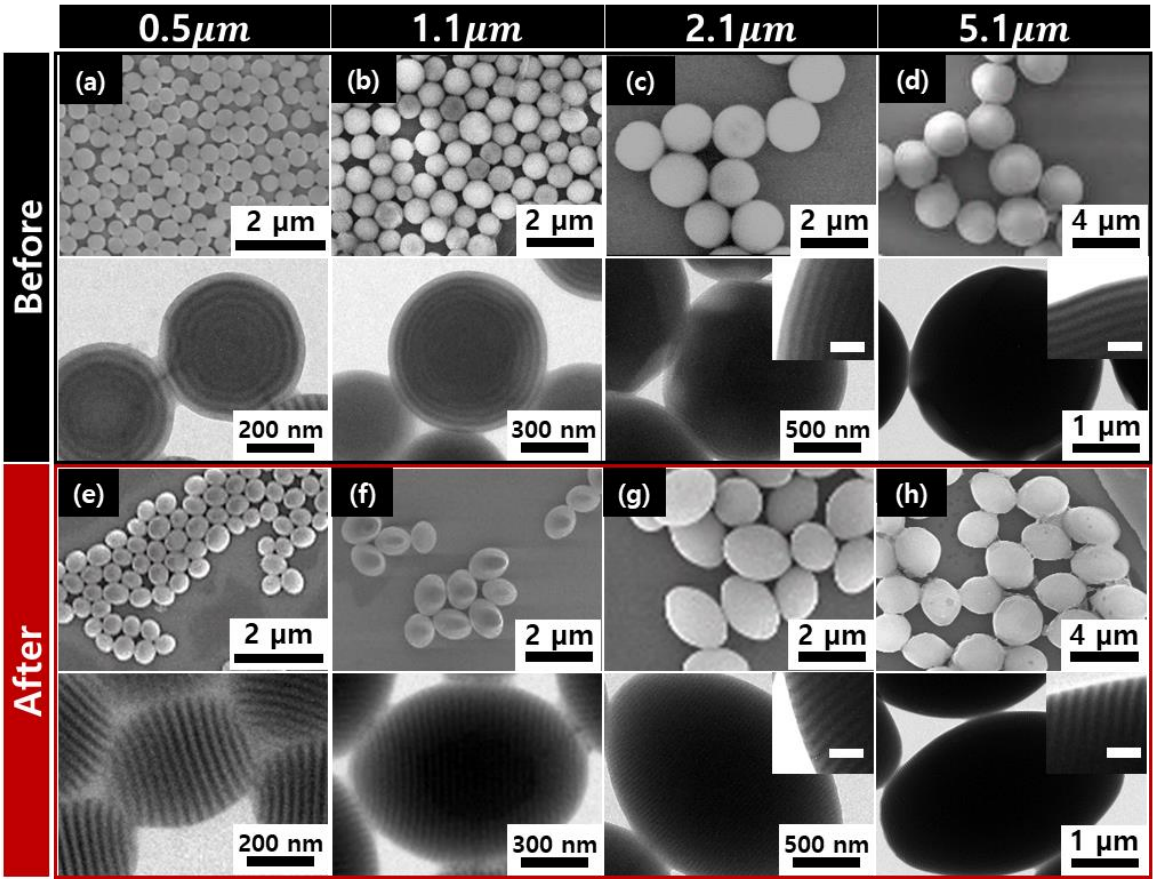

Figure S8. SEM and TEM images of (a-d) PS_{34k}-*b*-PB_{25k} spheres produced from membranes with d_{pore} = (a) 0.5, (b) 1.1 (c), 2.1 and (d) 5.1 μm. (e-h) The particles were transformed to prolate ellipsoids by PRSE. Scale bars in the insets (white) are 100 nm.

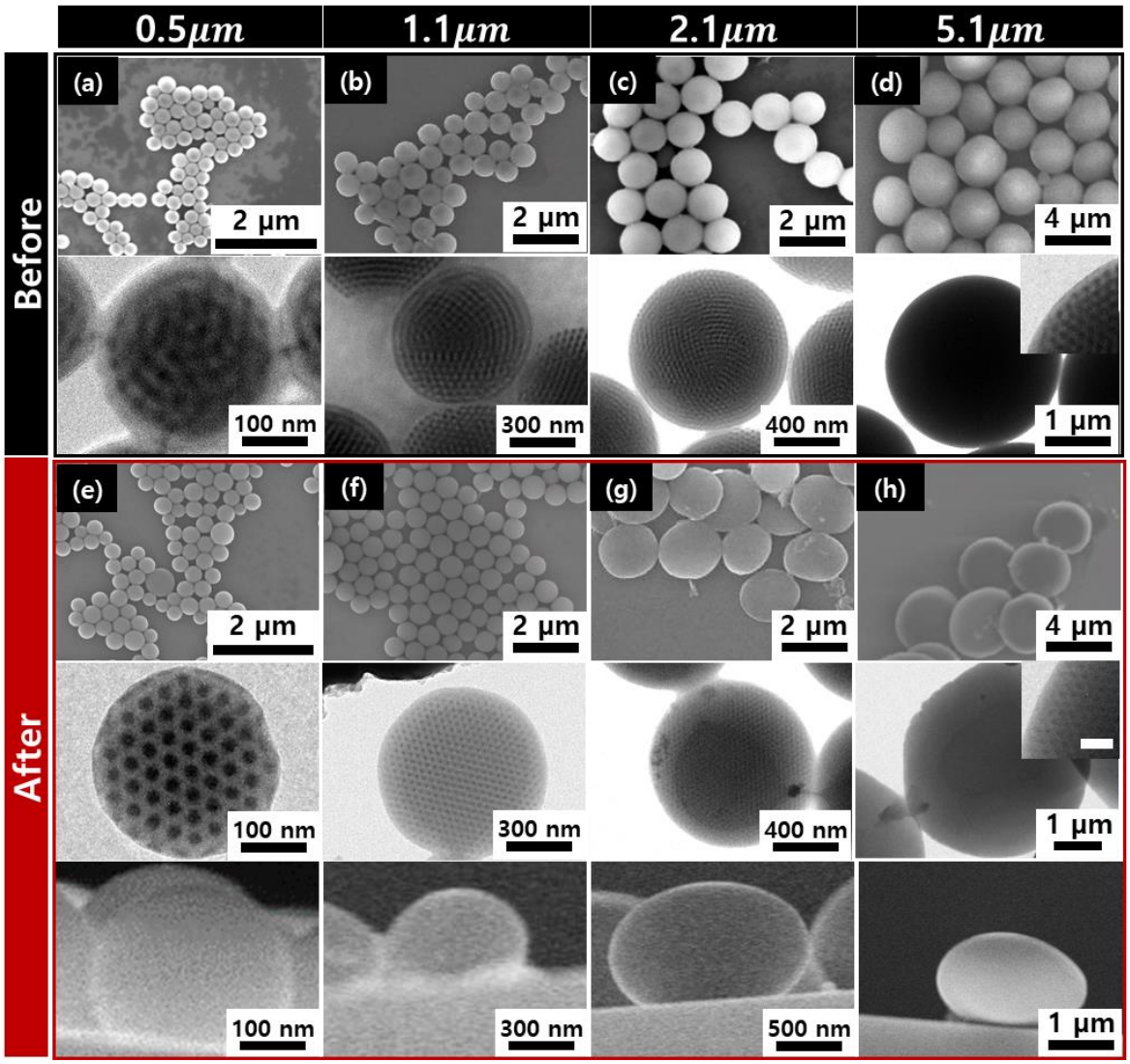

Figure S9. SEM and TEM images of (a-d) PS_{35k}-*b*-PB_{11k} spheres produced from membranes with d_{pore} = (a) 0.5, (b) 1.1, (c) 2.1 and (d) 5.1 μm. (e-h) The particles were transformed to oblate ellipsoids by PRSE. Scale bars in the insets (white) are 100 nm.

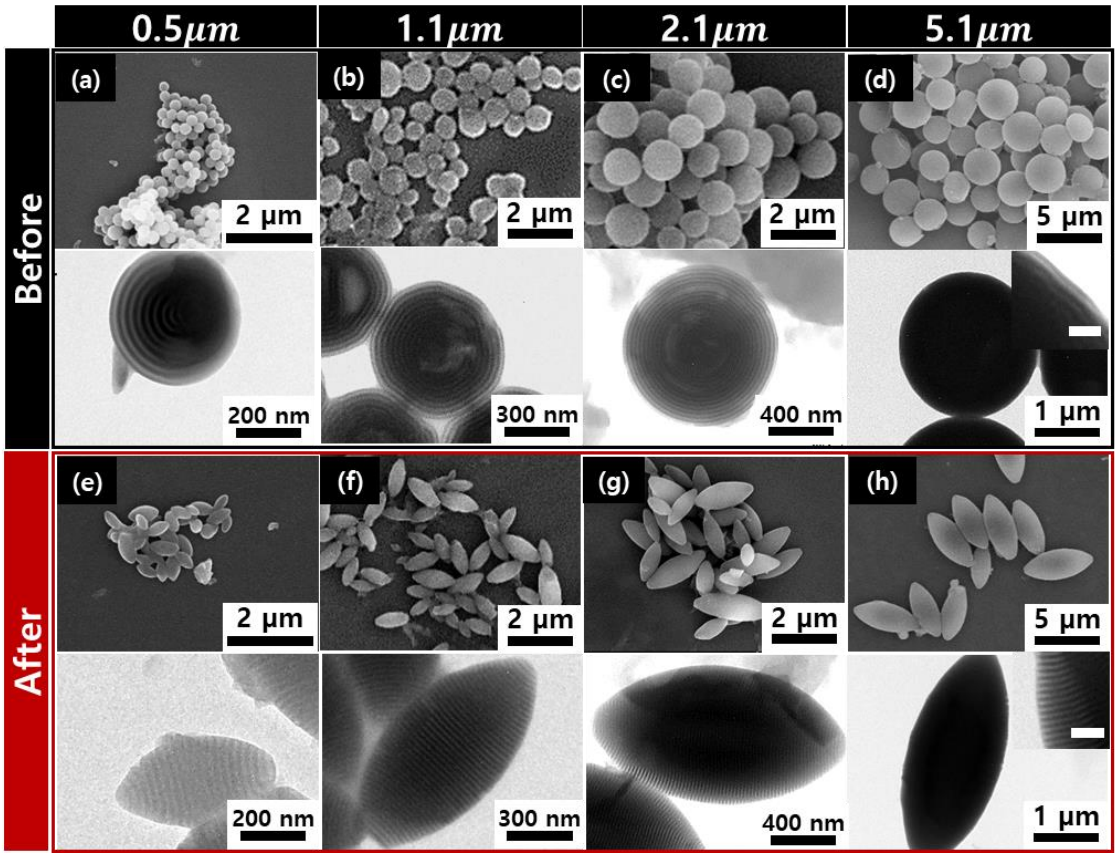

Figure S10. SEM and TEM images of (a-d) PS_{10k}-*b*-$P4VP_{10k}$ spheres produced from membranes with d_{pore} = (a) 0.5, (b) 1.1 (c), 2.1 and (d) 5.1 μm. (e-h) The particles were transformed to prolate ellipsoids by PRSE. Scale bars in the insets (white) are 100 nm.

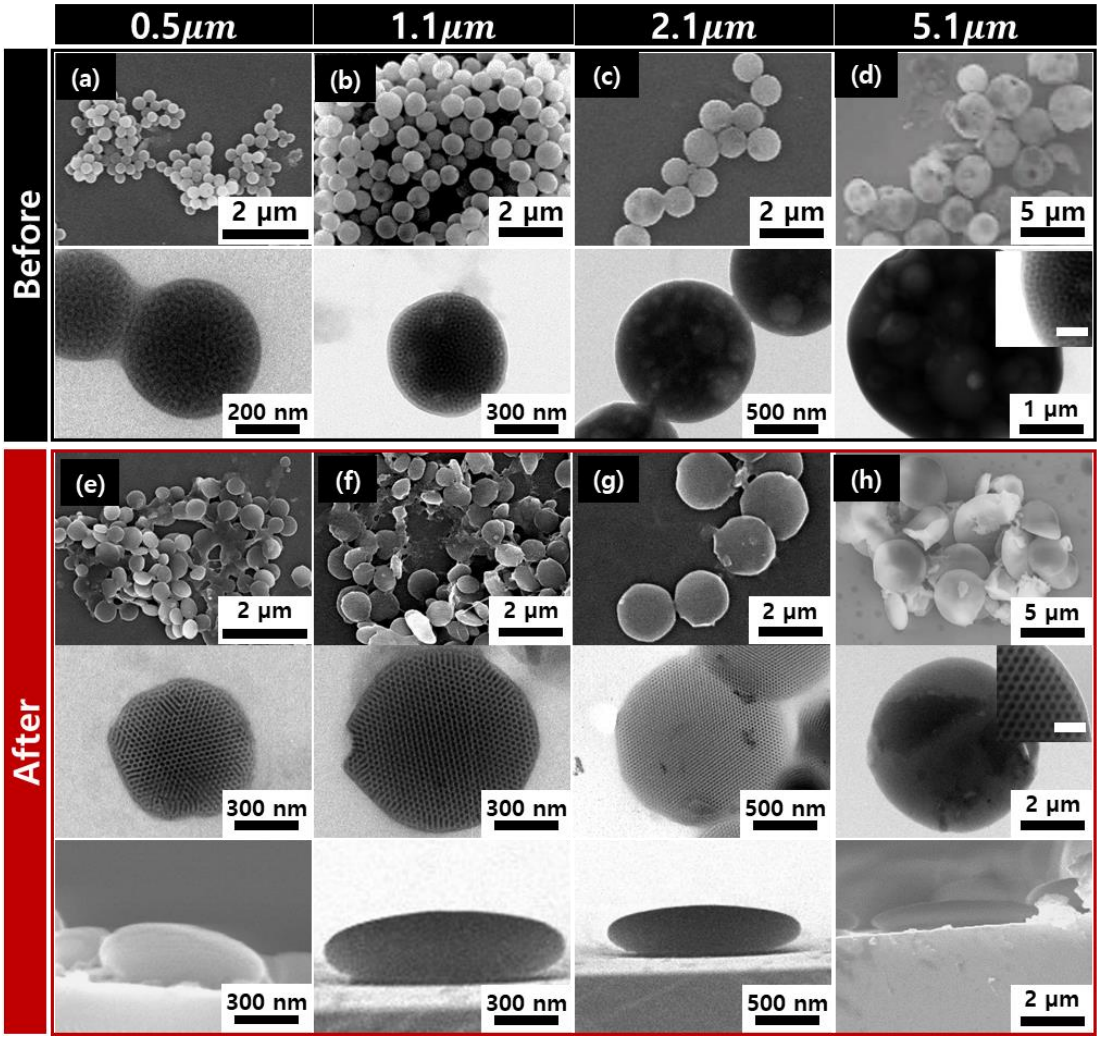

Figure S11. SEM and TEM images of (a-d) PS_{15k}-*b*-$P4VP_{7k}$ spheres produced from membranes with d_{pore} = (a) 0.5, (b) 1.1, (c) 2.1 and (d) 5.1 μm. (e-h) The particles were transformed to oblate ellipsoids by PRSE. Scale bars in the insets (white) are 100 nm.

Calculation Details for the AR of Prolate Ellipsoids

The total free energy of a prolate particle (F), with L and S as major and minor axis, consisting of n-layered A-b-B BCP lamellae from the center can be expressed as the following equation:

$$\frac{F}{k_bT} = \frac{(2n-1)\pi}{3b^2}\sqrt{\frac{\chi}{6}}S^2 + \frac{\pi^3L^3S^2}{192N^2b^5(2n-1)^2} + \frac{\pi^2L_0^4C^2V_c}{1024N^2b^5} + \frac{\pi[(1-f)\gamma_A + f\gamma_B]}{2(1+\beta\Sigma)^\alpha}S^2\left[1 + \frac{Lsin^{-1}\sqrt{1-S^2/L^2}}{S\sqrt{1-S^2/L^2}}\right] \quad \textbf{(S1)}$$

where k_b is the Boltzmann constant, T is temperature, χ is the incompatibility parameter of the BCP, b is monomer length, N is the degree of polymerization, f is volume fraction of BCP, γ_A is the interfacial tension between A-block and its surroundings, γ_B is the interfacial tension between B-block and its surroundings, and $\sum$ is the ratio of volume to surface area of the particle. α and β are fitting parameters for the surface energy term between BCPs and their surroundings. The first term in the right hand side of **equation S1** denotes the interfacial energy between the two blocks and the second term describes the chain stretching energy of the BCPs, assuming that the prolate particle consists of axially stacked lamellae. The third term describes the bending energies of curved lamellae at the edges (poles) of prolate ellipsoids,[7–9] where L_0 is bulk periodicity, C is curvature of the curved layers, and V_c is total volume of the curved layers. The last term is the surface energy between the BCPs and their surrounding medium. χ values were set to 0.04, 0.21, and 0.53 for PS_{34k}-b-PB_{25k}, PS_{16k}-b-$PDMS_{17k}$, and PS_{10k}-b-$P4VP_{10k}$, respectively.[10–13] For each BCP, the surface tension values between the polymer and its surroundings (γ_A) were set to γ_{PS} = 9.76 and γ_{PB} = 8.57 mN/m for PS_{34k}-b-PB_{25k}, γ_{PS} = 9.36 and γ_{PDMS} = 8.44 mN/m for PS_{16k}-b-$PDMS_{17k}$, and γ_{PS} = γ_{P4VP} = 10.54 mN/m for PS_{10k}-b-$P4VP_{10k}$ based on the contact angle measruements of each polymer film upon addition of water

containing surfactants. b was set to 0.6 for all BCPs. The free energy of the particle elongations becomes functions of n, L, S, α and β. Therefore, for each particle volume, the optimized set of L and S was numerically calculated by minimizing F. C and V_c were numerically calculated from the given geometry of the prolate particle. The fitting parameters were optimized to α =0.97 and β =0.90 for PS_{34k}-*b*-PB_{25k}, α =1.05 and β =0.80 for PS_{16k}-*b*-$PDMS_{17k}$, and α =1.10 and β =1.40 for PS_{10k}-*b*-$P4VP_{10k}$, respectively.

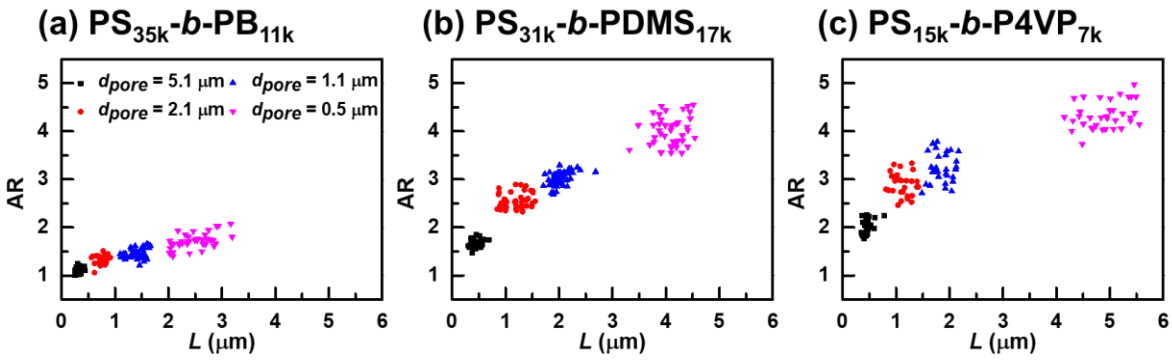

Figure S12. Plots of AR as a function of *L* of monodisperse oblate particles of (a) PS_{35k}-*b*-PB_{11k}, (b) PS_{31k}-*b*-$PDMS_{17k}$, and (c) PS_{15k}-*b*-$P4VP_{7k}$ after PRSE. Particles were produced from membranes with d_{pore} = 0.5, 1.1, 2.1, and 5.1 μm.

References

(1) Chu, L. Y.; Xie, R.; Zhu, J. H.; Chen, W. M.; Yamaguchi, T.; Nakao, S. I. Study of SPG Membrane Emulsification Processes for the Preparation of Monodisperse Core-Shell Microcapsules. *J. Colloid Interface Sci.* **2003**, *265*, 187–196.

(2) Cheng, C. J.; Chu, L. Y.; Xie, R. Preparation of Highly Monodisperse W/O Emulsions with Hydrophobically Modified SPG Membranes. *J. Colloid Interface Sci.* **2006**, *300*, 375–382.

(3) Calderara, F.; Riess, G.; Nationale, E.; Chimie, S. De; Werner, A. Characterization of Polystyrene-*block*-Poly (4-Vinyl- Pyridine) Block Copolymer Micelles in Toluene Solution. *Macromol. Chem. Phys.* **1996**, *197*, 2115–2132.

(4) Shin, J. M.; Kim, M. P.; Yang, H.; Ku, K. H.; Jang, S. G.; Youm, K. H.; Yi, G. R.; Kim, B. J. Monodispserse Nanostructured Spheres of Block Copolymers and Nanoparticles via Cross-Flow Membrane Emulsification. *Chem. Mater.* **2015**, *27*, 6314–6321.

(5) Schmidt, B. V. K. J.; Elbert, J.; Scheid, D.; Hawker, C. J.; Klinger, D.; Gallei, M. Metallopolymer-Based Shape Anisotropic Nanoparticles. *ACS Macro Lett.* **2015**, *4*, 731–735.

(6) Klinger, D.; Wang, C. X.; Connal, L. A.; Audus, D. J.; Jang, S. G.; Kraemer, S.; Killops, K. L.; Fredrickson, G. H.; Kramer, E. J.; Hawker, C. J. A Facile Synthesis of Dynamic, Shape-Changing Polymer Particles. *Angew. Chem. Int. Ed.* **2014**, *53*, 7018–7022.

(7) Wilmes, G. M.; Durkee, D. A.; Balsara, N. P.; Liddle, J. A. Bending Soft Block Copolymer Nanostructures by Lithographically Directed Assembly. *Macromolecules* **2006**, *39*, 2435–2437.

(8) Wang, Z. G. Response and Instabilities of the Lamellar Phase of Diblock Copolymers under Uniaxial Stress. *J. Chem. Phys.* **1994**, *100*, 2298–2309.

(9) Wang, Z. G.; Safran, S. A. Curvature Elasticity of Diblock Copolymer Monolayers. *J. Chem. Phys.* **1991**, *94*, 679–687.

(10) Jin, H. M.; Park, D. Y.; Jeong, S. J.; Lee, G. Y.; Kim, J. Y.; Mun, J. H.; Cha, S. K.; Lim, J.; Kim, J. S.; Kim, K. H.; et al. Flash Light Millisecond Self-Assembly of High χ Block Copolymers for Wafer-Scale Sub-10 nm Nanopatterning. *Adv. Mater.* **2017**, *29*, 1–7.

(11) Men'shikov, E. A.; Bol'shakova, A. V.; Yaminskii, I. V. Determination of the Flory-Huggins Parameter for a Pair of Polymer Units from AFM Data for Thin Films of Block Copolymers. *Prot. Met. Phys. Chem. Surfaces* **2009**, *45*, 295–299.

(12) Nunns, A.; Gwyther, J.; Manners, I. Inorganic Block Copolymer Lithography. *Polymer* **2013**, *54*, 1269–1284.

(13) Stadler, R.; Auschra, C.; Beckmann, J.; Krappe, U.; Voigt-Martin, I.; Leibler, L. Morphology and Thermodynamics of Symmetric Poly(A-*block*-B-*block*-C) Triblock Copolymers. *Macromolecules* **1995**, *28*, 3080–3097.